# Calculation of Flow Over Iced Airfoils

Tuncer Cebeci*
*California State University, Long Beach, California*

**Progress toward the development of a method for predicting the flowfield of an iced airfoil is described and shown to offer the prospect of a priori calculations of the effects of ice accretion and roughness on airfoil performance. The approach is based on interaction of inviscid flow solutions obtained by a panel method and improved upon by a finite-difference boundary-layer method that, operating in an inverse mode, incorporates viscous effects, including those associated with separated flows. Results are presented for smooth, rough, and iced airfoils as a function of angle of attack. Those for smooth and rough airfoils confirm the accuracy of the method and its applicability to surfaces with roughness similar to that associated with insect deposition and some forms of ice. Two procedures have been developed to deal with large ice accretion and their performance is examined and shown to be appropriate to the engineering requirements.**

## I. Introduction

ACCORDING to experiments, including those of Refs. 1-6, ice accretion on airfoils may affect their aerodynamic characteristics by reducing $C_{\ell max}$ drastically and increasing drag substantially. In general, two classes of ice accretion, known as rime and glaze, occur under different flight conditions. Rime ice is formed at low air temperatures and velocities, where supercooled water droplets freeze on impact, and is usually encountered in flight through clouds with low liquid-water content. Glaze ice can have a stronger influence on the lift and drag and occurs at temperatures just below freezing when water droplets flowing along the surface freeze to form ice horns.

The influence of ice accretion on the aerodynamic properties of airfoils has been investigated experimentally over many years. Early results were reported by Gray and Von Glahn,[1] who examined NACA 65-212 and 65A004 airfoils and showed the adverse effects of ice on airfoil performance. Bragg et al.,[2,3,5-7] Bragg,[8] and Korkan et al.[9] investigated the effects of simulated ice shapes on integrated lift, drag, and moments and provided information on the length of separation bubbles, reattachment, and trailing-edge separation. The flow visualization experiments of Bragg[8] showed the separation bubbles associated with glaze ice in terms of photographs of oil flow on a splitter plate for two different glaze ice shapes at two angles of attack.

In their study of iced airfoils, Bragg and Coirier[5] simulated a glaze-ice accretion on a 21 in. chord model NACA 0012 airfoil and reported measurements of surface pressures, lift and moment coefficients, and airfoil drag. The separation bubble was explored by measuring the time-averaged velocities using a split-film probe and measurements were made with and without the simulated glaze ice. Velocity profiles in the separation bubble were presented for several chordwise stations at three angles of attack and the results indicate that the ice shape caused a severe reduction in lift and a substantial increase in drag. The velocity profiles show clearly the large regions of reversed flow and bubble reattachment. This work was extended by Bragg and Spring,[6] who used similar techniques to investigate the influence of roughness on iced airfoils. As expected, the effect of the roughness proved to be much less than that of large glaze-ice accretions, although it can be important where the accretion is small. The data presented in Ref. 6 add considerably to that of Ref. 5.

Early attempts to represent the effects of ice by correlation formulas included that of Ref. 1 and were based on data collected in the NASA Lewis Icing Research Tunnel. These data are best suited for glaze conditions, and a correlation given in Ref. 10 shows that it provides guidance, although the predicted drag rise is often too large. Flemming and Lednicer[11] acquired a large data base in the Canadian NRC high-speed icing wind tunnel for a series of reduced-scale rotor airfoil sections and provided a correlation for two airfoils, also discussed in Ref. 10.

It is clear from these correlations and from additional examples cited in Ref. 10 that the experimental data involve effects not represented by the correlation equations. They are confined mainly to drag and do not include terms to take account of known effects such as Reynolds number, airfoil shape, and slats. There is a clear need for a procedure that will calculate the aerodynamic properties of the flow around airfoils with correct representation of the large changes in geometry associated with accretions of rime and glaze ice. The present investigation was undertaken to meet this need and is based on an interactive boundary-layer method, previously developed to represent the flow over clean airfoils for a wide range of angles of attack up to and including stall.[12] A separate study, based on the solution of thin Navier-Stokes equations in a body-fitted curvilinear coordinate system, is being carried out by Potapczuk.[13,14] These two approaches form part of a more extensive program of research initiated and coordinated by NASA Lewis Research Center with the purpose of developing computer codes so as to permit the prediction of ice formation and its aerodynamic consequences. A full description of this effort has been provided by Shaw[10,15,16] and includes consideration of particle trajectories and the mechanism of ice accretion, methods of avoiding and removing accretions of ice, and the consequences of ice accretion for aerodynamic performance.

The calculation method is described briefly in Sec. II, with further information available in Refs. 12 and 17. The calculated results are presented in the three subsections of Sec. III dealing with smooth airfoils, rough airfoils, and iced airfoils, respectively. The first subsection is included to quantify the extent to which the present method and one based on the solution of the thin-layer Navier-Stokes equations can represent airfoil flows as a function of angle of attack without the added complication of a roughened surface. The rough surfaces described in Sec. III.B allow examination of the value of the concept of equivalent sand-grain roughness within the framework of the turbulence model of the interactive proce-

Received Dec. 2, 1987; presented as Paper 88-0112 at the AIAA 26th Aerospace Sciences Meeting, Reno, NV, Jan. 11-14, 1988; revision received June 27, 1988. 

*Professor and Chairman, Aerospace Engineering Department. Fellow AIAA.

dure and show the accuracy of computing flows over iced airfoils where the ice can be considered as roughness. Section III.C describes results obtained with two separate procedures developed for the leading-edge region in order to cope with the drastic geometry changes caused by the ice shapes. Summary conclusions are identified in Sec. IV.

## II. Calculation Method

The interactive boundary-layer method described by Cebeci et al.[12] provides the foundation for the present work. It comprises solution procedures for inviscid flow and boundary-layer equations and a procedure that couples them together so as to ensure that each influences the other. The boundary-layer solution procedure is based on Keller's box scheme and the finite-difference approximations are written for conservation equations expressed in terms of Falkner-Skan variables. The eddy-viscosity formulation of Ref. 18 is used in regions of transitional and turbulent flow and the onset of turbulence is specified by the expression of Ref. 19 or by the occurrence of laminar separation. These features of the method are outlined in Sec. II.A, with a more complete description of the procedures used to deal with the nonaerodynamic nature of ice accretions in Sec. II.C. The modifications required to deal with surface roughness are described briefly in Sec. II.B.

### A. Interactive Boundary-Layer Method

Studies with conformal mapping and panel methods showed that the latter were more suitable for the geometrical arrangements of ice and the present panel method defines the airfoil and ice by a set of points in the physical plane. Neighboring points are connected by straight-line panels, each of which has source density and vorticity. The vorticity strength of each panel is the same so that vorticity is defined by a total strength, adjusted to satisfy the Kutta condition. The source strengths have independent values on each panel, and these are adjusted, by solving a set of simultaneous linear equations, to satisfy the normal-velocity boundary condition at the midpoints of the panels. In the strictly inviscid case, this condition requires that the total normal velocity, freestream plus body sources and vortices, should vanish. When the boundary layer is simulated, the desired normal velocity $v_n$ is finite and equals the derivative along the surface of the product of tangential velocity and displacement thickness, $d/ds\ (u_e\delta^*)$. It is shown that this surface blowing distribution displaces the dividing streamline outward from the surface of the airfoil to the location of the displacement thickness. Experience has shown that best results are obtained when surface pressures are calculated and the Kutta condition applied on the displacement surface rather than on the surface panels.

The boundary-layer equations for two-dimensional external steady incompressible flows are well known and are solved here with the external velocity distribution $u_e(x)$ obtained from inviscid flow theory. With $u_e^0(x)$ denoting the inviscid velocity distribution and $\delta u_e(x)$ the perturbation velocity due to viscous effects,

$$u_e(x) = u_e^0(x) + \delta u_e(x) \tag{1}$$

$$\delta u_e(x) = \frac{1}{\pi}\int_{x_a}^{x_b} \frac{\mathrm{d}}{\mathrm{d}\sigma}(u_e\delta^*)\frac{\mathrm{d}\sigma}{x-\sigma} \tag{2a}$$

where $\mathrm{d}(u_e\delta^*)/\mathrm{d}\sigma$ is the blowing velocity and the interaction is confined to the range $x_a \le x \le x_b$.

In this form, Eq. (2a) provides an outer boundary condition for the viscous flow calculations that represent the viscous/inviscid interaction and can be generalized to the form[12]

$$u_e(x) = u_e^\kappa(x) + \sum_{j=1}^{n} c_{ij}[(u_e\delta^*)_j - (u_e\delta^*)_j^\kappa] \tag{2b}$$

where $u_e^\kappa(x)$ corresponds to the inviscid velocity distribution containing the displacement thickness effect $(\delta^*)^\kappa$ computed from a previous sweep. Here $c_{ij}$ denotes the interaction-coefficient matrix, which is obtained from a discrete approximation to the Hilbert integral.

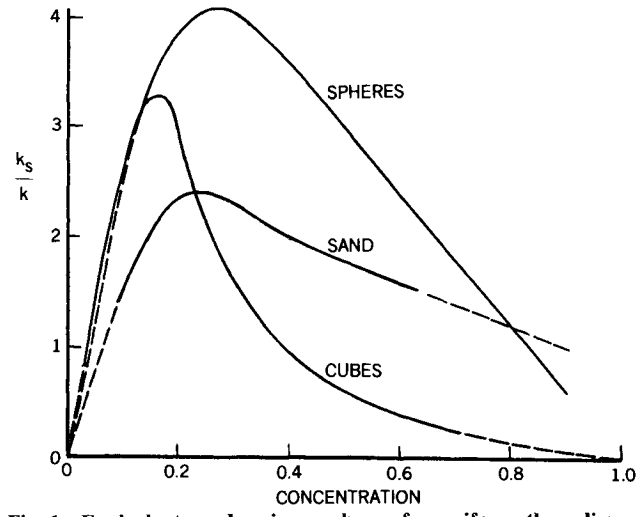


**Fig. 1 Equivalent sand-grain roughness for uniform three-dimensional roughness as a function of concentration (dashed lines are extrapolations of experimental data).**

The numerical solution of the boundary-layer equations, written in transformed variables, are obtained with Keller's box method for both standard (given pressure distribution) and interactive methods. This second-order finite-difference method has been used extensively by Cebeci and his associates for a wide range of flows. As in previous studies, an inverse form of the equations is used to obtain the solutions with separation and, as before, the FLARE approximation, in which the convective term $u(\partial u/\partial x)$ is set equal to zero in the recirculating region, is employed. No attempt was made to improve the accuracy of the solutions resulting from this approximation. The nonlinear system of algebraic equations that results from the finite-difference approximations is linearized by Newton's method and solved by a block elimination procedure. Complete details of this procedure are described in Ref. 20.

### B. Surface Roughness

To extend the calculation method to deal with rough surfaces, the experiments of Ref. 21 were represented by the interactive boundary-layer method. The roughness comprised 0.001 in. carborundum grains applied to 24 in. chord airfoils and spread evenly over a surface length of 0.08 chord. Within the framework of the turbulence model of Cebeci and Chang,[22] the mixing length expression used in the Cebeci-Smith model[18] was modified as

$$L = \kappa(y + \Delta y)\{1 - \exp[-(y + \Delta y)/A]\}$$

where $\Delta y$ is a function of an equivalent sand-grain roughness $k_s$. In terms of dimensionless quantities with $k_s^+ = k_s u_\tau/\nu$ and $\Delta y^+ = \Delta y u_\tau/\nu$, we have

$$\Delta y^+ = 0.9[\sqrt{k_s^+} - k_s^+ \exp(-k_s^+/6)] \quad 5 < k_s^+ \le 70$$

$$= 0.7(k_s^+)^{0.58} \quad 70 \le k_s^+ \le 2000$$

In order to convert the roughness corresponding to carborundum grains into equivalent sand-grain roughness, we used the procedure of Smith and Kaups[23] in which the ratio of the equivalent sand-grain roughness to the roughness of the applied elements, $k_s/k$, was assumed to be a function of the concentration and shape of the roughness elements; see Fig. 1. In all cases considered here, the shape of the elements was approximated by a sphere; the concentration, which represents the mean value of the area covered by the roughness elements, was taken as 0.075 and the equivalent sand-grain roughness height was obtained from Fig. 1 as $k_s/c = 0.00094$.

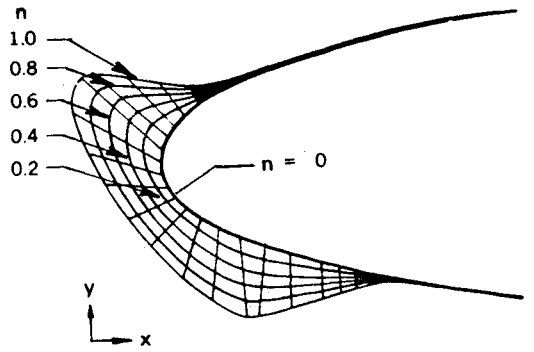


**Fig. 2 Ice shapes used in the first continuation method ($n$ = 1 corresponds to the prescribed shape).**

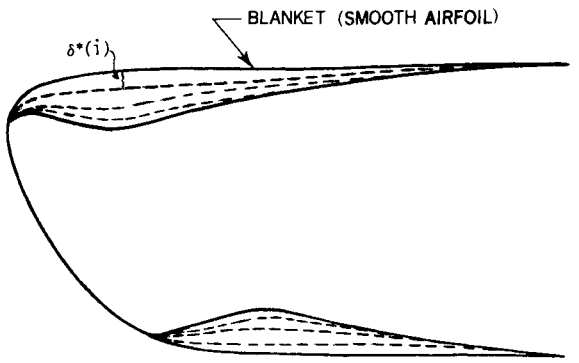


**Fig. 3 Ice shapes used in the second continuation method.**

### C. Procedures to Deal with Leading-Edge Ice Shapes

Ice on airfoils can introduce drastic geometric changes to their leading edges and cause rapid variations in the flow properties. As a result, the inviscid and viscous flow calculations may have difficulty in producing satisfactory solutions. Depending on the ice shape, local regions of flow separation can occur and influence the lift and drag characteristics of the airfoil.

Two separate procedures have been developed to reduce the sensitivity of the calculations caused by the leading-edge ice. The first procedure makes use of a continuation method in which the prescribed ice shape is gradually introduced into the calculations. Figure 2 shows a sketch of the iced airfoil in which the ice shape changes in increments of $n$ ranging from 0–1, with $n = 0$ corresponding to the clean airfoil and $n = 1$ to the airfoil with the prescribed ice shape. The calculations in this case start with a clean airfoil ($n = 0$) for an angle of attack $\alpha = 0$. A series of inviscid and viscous flow calculations then are performed in the spirit of the interactive boundary-layer procedure. After the convergence of the solutions, the ice shape is introduced into the calculations by taking an incremental value of $n$ and again iterating the solutions until convergence. Subsequent calculations then are made in increments of $n$ up to $n = 1.0$. Once a converged solution for $\alpha = 0$ is obtained in this manner, the calculations for another angle of attack are performed for $n = 1$ by initially computing the pressure distribution for the new angle of attack from the blowing velocity of the iced airfoil at the previous angle of attack. With each solution of the boundary-layer equations, a new blowing velocity is computed to obtain a new pressure distribution and, as before, this procedure is continued until convergence. At small angles of attack, it is sufficient to choose the increments $\delta\alpha$ to be around 0.50 deg; at higher angles, especially at conditions approaching stall, $\delta\alpha$ had to be smaller, becoming around 0.1 deg for $\alpha$ of 5–6 deg. The results obtained with this procedure are discussed in Sec. III.C.

The second procedure treats the iced airfoil as a smooth surface obtained by covering the leading-edge region with a "blanket" as shown in Fig. 3. It also makes use of a continuation method in that the initial calculations are performed for the "smooth" airfoil and subsequent ones for a series of shapes that fall between the smooth and iced airfoils. For each shape, the blowing velocity is computed from

$$v_n = \frac{\mathrm{d}}{\mathrm{d}x}\left[u_e(\delta^* - \delta)\right]$$

where $\delta^*$ corresponds to the displacement thickness obtained from the boundary-layer solutions for the shape whose geometrical difference from the smooth airfoil is $\delta^{(i)}(x)$ and where the $\delta^*$ surface is outside the singularity surface. As in the first procedure, this allows the viscous effects to be incorporated into the inviscid flow solutions gradually, thus reducing the sensitivity of the viscous flow solutions to the rapid changes in the pressure distribution near the leading edge. Computed results with this procedure also are presented in Sec. III.C.

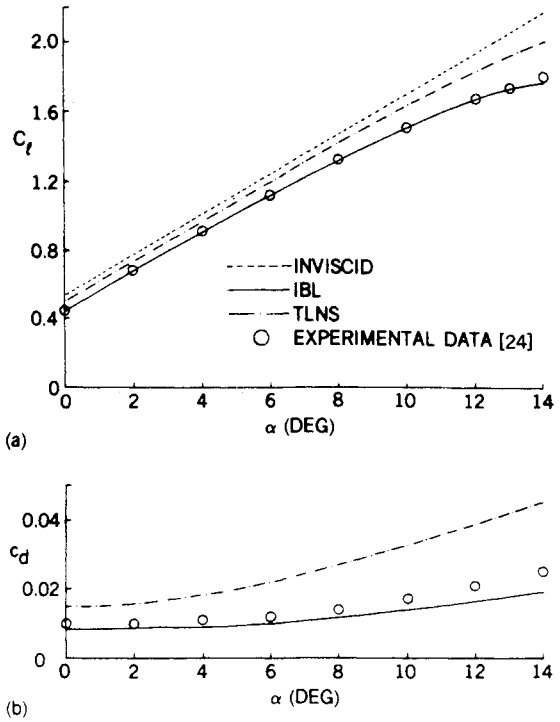


**Fig. 4 Variation of lift and drag coefficients for the GA(W)-2 airfoil ($R_c = 4.3 \times 10^6$).**

## III. Results and Discussion

The interactive boundary-layer procedure described in the previous section is general and is applicable to airfoils with a range of surface conditions. Results for clean and rough airfoils are presented in the following two subsections. For clean airfoils, the predictions of the interactive boundary-layer method also are compared with those obtained from the solutions of the thin-layer Navier-Stokes code (ARC 2D) as well as with the experimental data. The predictions of rough airfoils are obtained only with the interactive boundary-layer approach, and it is expected that similar results can be obtained from the solution of the thin-layer equations. The third subsection describes results obtained with the two procedures developed to handle the geometric difficulties introduced by ice shapes.

### A. Smooth Airfoils

Figure 4 presents results obtained with the interactive and thin-layer Navier-Stokes procedures for the GA(W)-2 airfoil for a range of angles of attack up to around 14 deg. It is taken from Ref. 17, from which additional results can be obtained. As can be seen, the predictions of the two calculation methods for this 13% thick airfoil represent an improvement over the

inviscid flow calculations in terms of the lift coefficient. As before, the interactive scheme provides results in very close agreement with experiment[24] and is also able to calculate the drag coefficient with accuracy that diminishes with angle of attack so that the difference between measurement and calculation is around 20% at 14 deg. The results of the thin-layer Navier-Stokes method (TLNS) are less satisfactory. A sample of pressure distributions provided in Ref. 17 shows the need for proper implementation of this method in the trailing-edge region.

Figures 5 and 6 show the calculated results for the NACA 0012 airfoil at a chord Reynolds number of $1.5 \times 10^6$ together with the measurements of Bragg and Spring.[6] As can be seen from Fig. 5, the lift coefficients are in close agreement with experiment up to the angle of attack that corresponds to $C_{\ell max}$ and the drag coefficients show very similar trends. Drag coefficients calculated with transition fixed at 5% chord agree better with experimental data than those corresponding to natural transition. In this case, the location of transition needed in the calculations was determined by Michel's formula[19] or by the onset of laminar separation. The calculated velocity profiles for $\alpha = 0$ and 4 deg shown in Fig. 6 also indicate an excellent agreement with measurements.

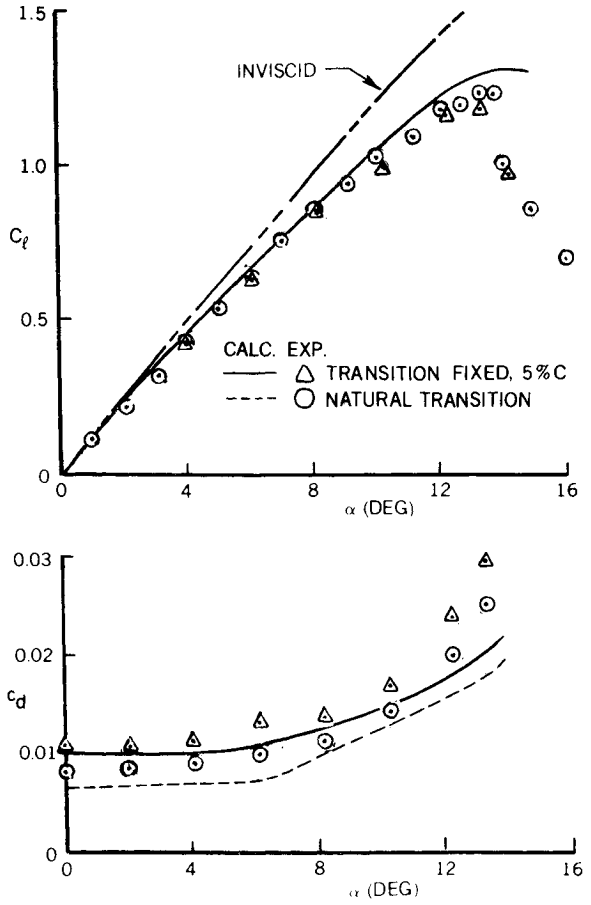


**Fig. 5 Results for the clean airfoil of Bragg and Spring.[6]**

### B. Rough Airfoils

The expression of Sec. II.B was used for three airfoils (NACA 4412, 23012, and 0012) for which experiments were performed[21] at a Reynolds number of $R_c = 6 \times 10^6$.

Figure 7 shows the results for the NACA 4412 airfoil. It can be seen from the lift coefficient results of Fig. 7a that the computations and measurements agree well up to the stall angles for the smooth airfoil as well as for the airfoil with leading-edge roughness. The drag curves of Fig. 7b also show good agreement between computations and measurements, although for the clean airfoil the drag is slightly underpredicted at higher angles of attack.

The NACA 23012 airfoil, like the NACA 4412, has camber, and the results of Fig. 8 again demonstrate good agreement between the computations and measurements. The drag curve is in even better agreement than that for the NACA 4412. These results, together with those shown in Fig. 9 for the NACA 0012 airfoil, quantify the extent to which the interactive boundary-layer method can represent the flows over airfoils with roughened surfaces. It is evident that the calculation method correctly represents this effect and the trends of the lift and drag curves. Where the effects of ice, rain, or insect deposition can be regarded as roughness with an equivalent sand-grain value, similar results can be expected.

### C. Iced Airfoils

The calculations for the iced airfoil were performed with the two procedures described in Sec. II.B. In the first procedure, in which the ice shape was changed according to Fig. 2, the viscous wake effect was neglected and the viscous flow calculations were performed only up to the trailing edge. Studies on smooth airfoils have shown that this procedure is reasonable as long as there is no or very small separation in the trailing-edge region of the airfoil. For this reason, we expect the iced airfoil calculations to be more accurate at small-to-moderate angles of attack than those at high angles of attack.

The experimental data on the iced airfoil[5] was obtained at a Reynolds number of $1.5 \times 10^6$, and a large change in the leading edge was arranged with a wooden attachment to represent the shape of a typical glaze-ice formation.

Before we present the results for this iced airfoil obtained with the first procedure of Sec. II.B, however, it is instructive to examine the inviscid external velocity distribution near the leading edge. As can be seen from Fig. 10, this distribution differs with and without ice: the clean airfoil has a favorable pressure gradient followed by an almost zero pressure gradient, whereas the iced airfoil has a severe adverse pressure gradient after a short initial region of favorable pressure gradient. For both surfaces, the rapid flow deceleration is followed by a

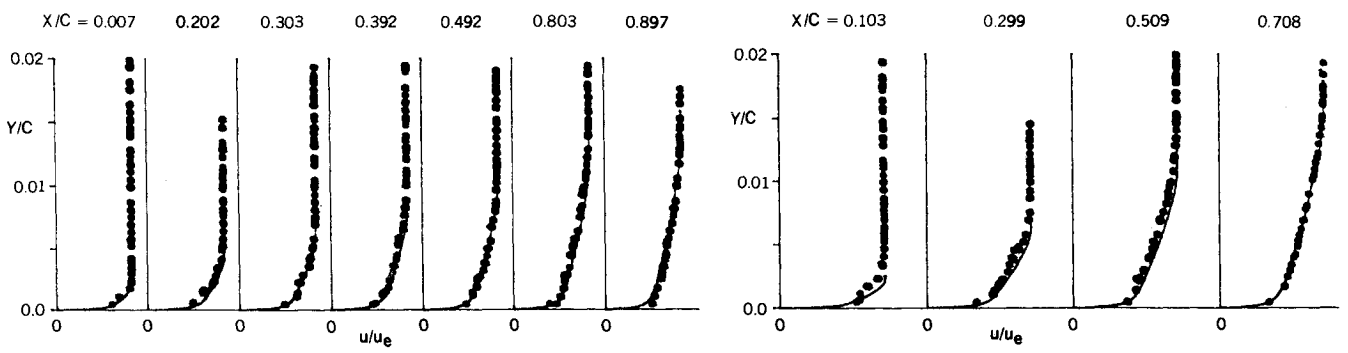


a) $\alpha = 0$ deg b) $\alpha = 4$ deg

**Fig. 6 Results for the clean airfoil of Bragg and Spring.[6]**

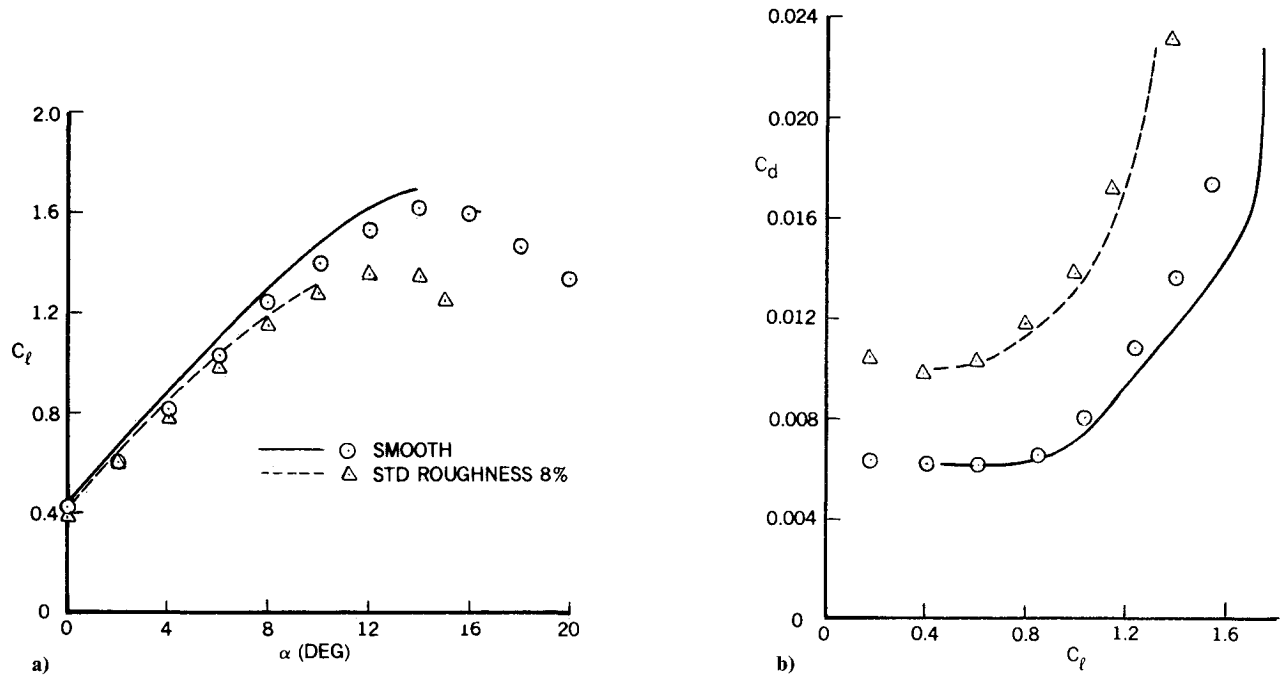


Fig. 7 Comparison of calculated and experimental results for the NACA 4412 airfoil at $R_c = 6 \times 10^6$.

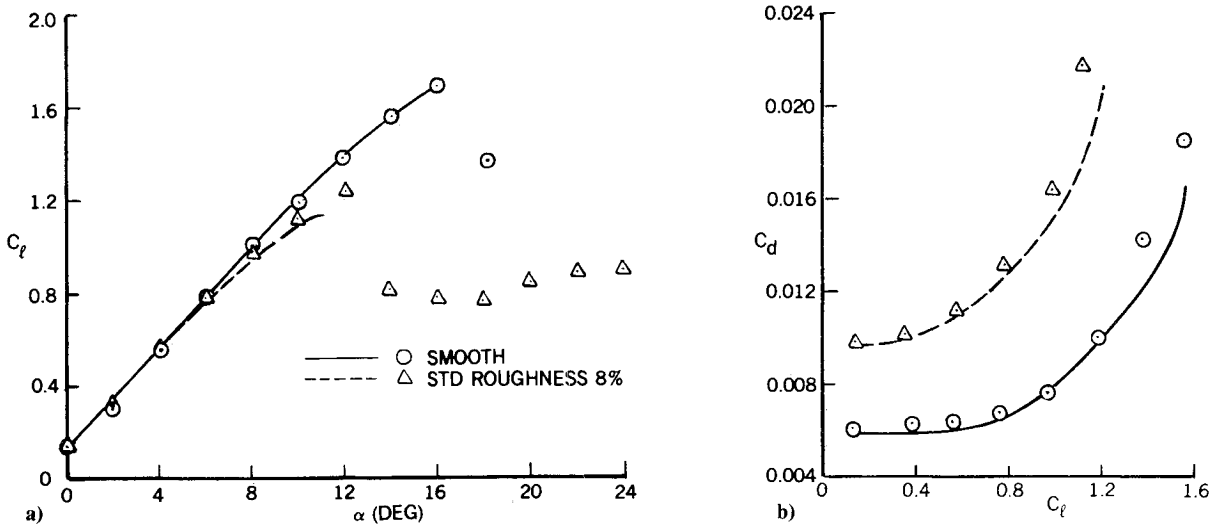


Fig. 8 Comparison of calculated and experimental results for the NACA 23012 airfoil at $R_c = 6 \times 10^6$.

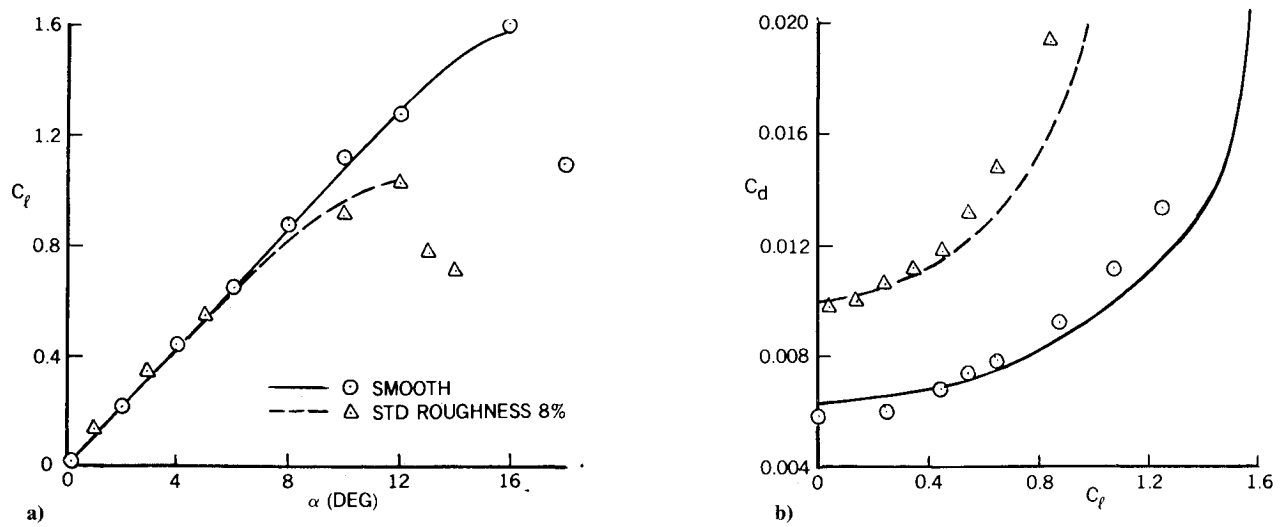


Fig. 9 Comparison of calculated results for the NACA 0012 airfoil at $R_c = 6 \times 10^6$.

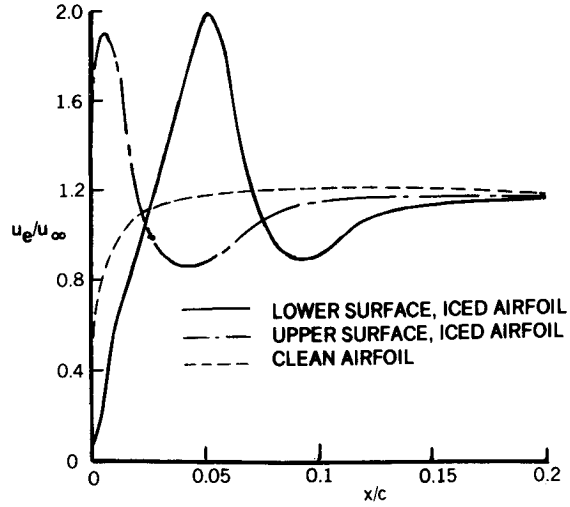


**Fig. 10 Inviscid $u_e/u_\infty$ distributions for iced and clean NACA 0012 airfoil at $\alpha = -0.15$ deg.**

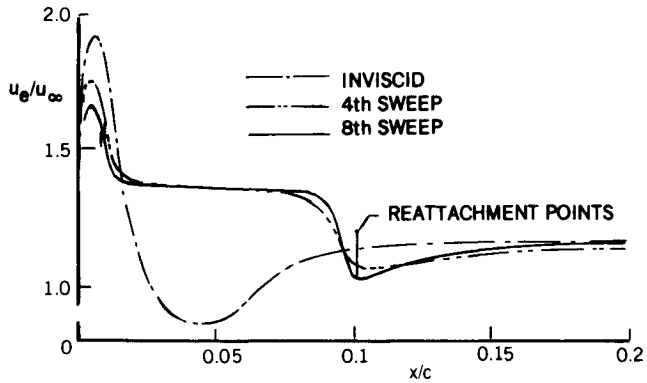


a) Upper surface

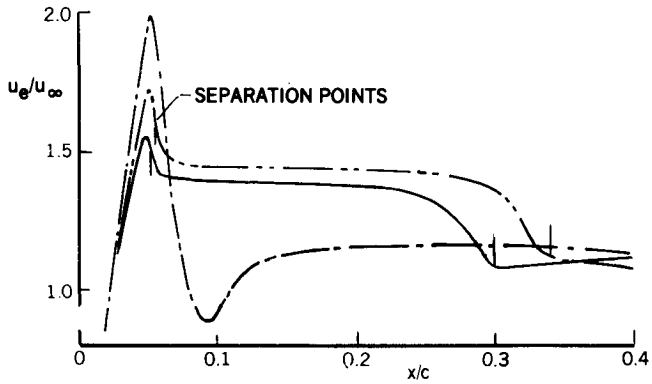


b) Lower surface

**Fig. 11 Variation of external velocity distribution on iced NACA 0012 airfoil with each boundary-layer sweep for $\alpha = -0.15$ deg and $R_c = 1.5 \times 10^6$.**

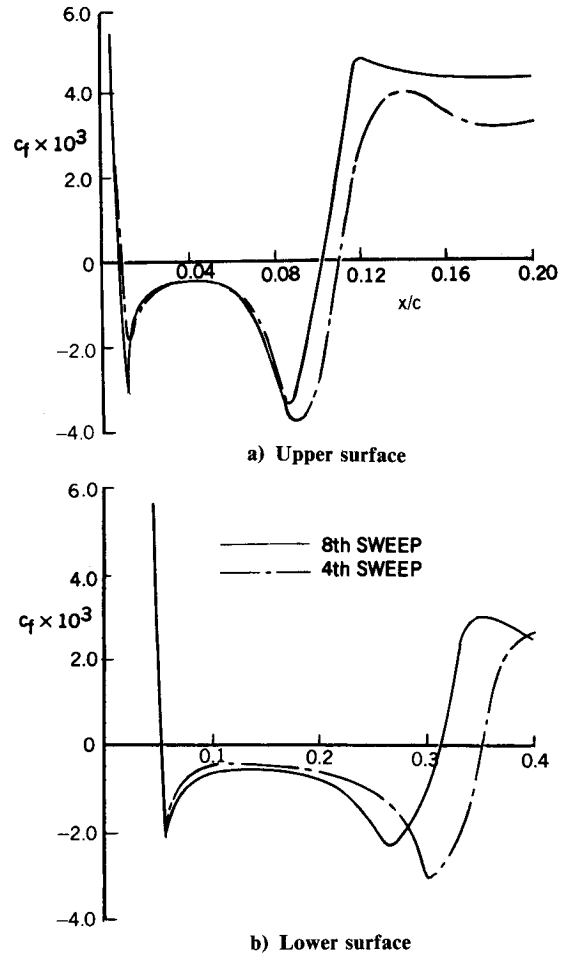


a) Upper surface

b) Lower surface

**Fig. 12 Variation of local skin-friction coefficient distribution on iced NACA 0012 airfoil with each boundary-layer sweep for $\alpha = -0.15$ deg and $R_c = 1.5 \times 10^6$.**

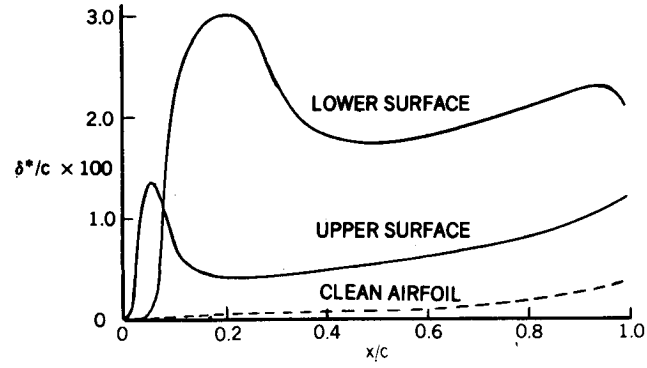


**Fig. 13 Displacement thickness distributions for clean and iced NACA 0012 airfoil at $\alpha = -0.15$ deg and $R_c = 1.5 \times 10^6$.**

gentle favorable pressure gradient and the locations of possible flow separation are easily identified.

The results of Figs. 11 and 12 were obtained with the interactive boundary-layer procedure and were begun at the stagnation point. Figure 11 shows the substantial difference between the initial inviscid flow calculation, which corresponds to that of Fig. 10, and the interactive result after four sweeps. The freestream velocity obtained from the eighth sweep may be regarded as converged. The results of Figs. 11 and 12 indicate a 10% chord separation bubble for the upper surface and a 25% chord separation bubble for the lower surface. Unlike the separation point, the reattachment point moves upstream with each sweep, but the difference in reattachment points becomes smaller with increase in the number of sweeps.

Perhaps the biggest surprise in the interactive flow calculations is the behavior of the displacement thickness distribution on the airfoil. Since the incidence angle is practically zero and the airfoil is symmetrical, the displacement thickness distributions on both surfaces are the same for the clean airfoil. Its magnitude at the trailing edge is approximately 0.5% of the airfoil chord, which is relatively small and has a very small effect on the overall pressure distribution. In the case of the iced airfoil, the flow separation due to ice alters the displacement thickness distribution on the airfoil (Fig. 13) so that the lower surface has a large separation bubble, which causes the magnitude of the displacement thickness at the trailing edge to be about 2% of the airfoil chord. The upper surface has a smaller separation bubble and the displacement thickness at

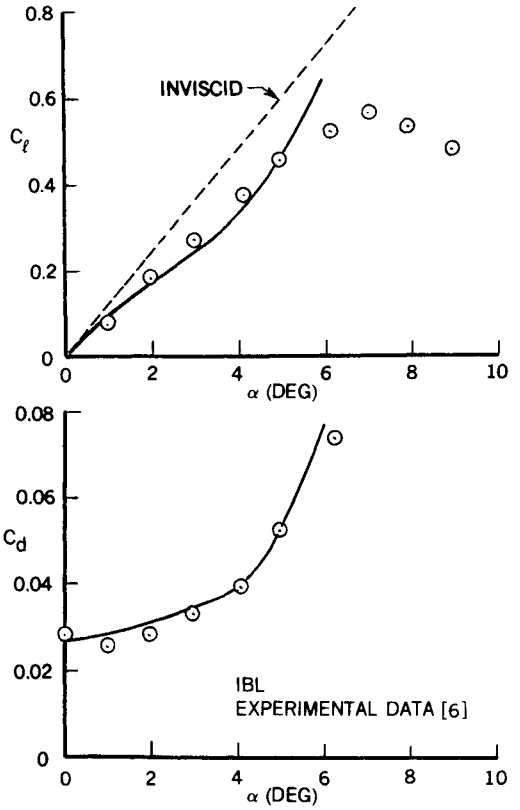


**Fig. 14 Calculated and experimental results for the iced NACA 0012 airfoil, $R_c = 1.5 \times 10^6$ (first procedure with no wake effect).**

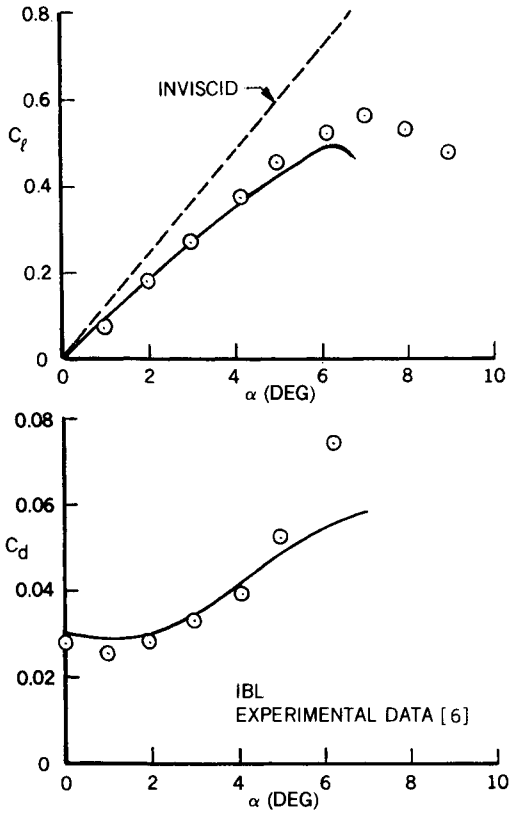


**Fig. 15 Calculated and experimental results for the iced NACA 0012 airfoil, $R_c = 1.5 \times 10^6$ (second procedure with wake effect).**

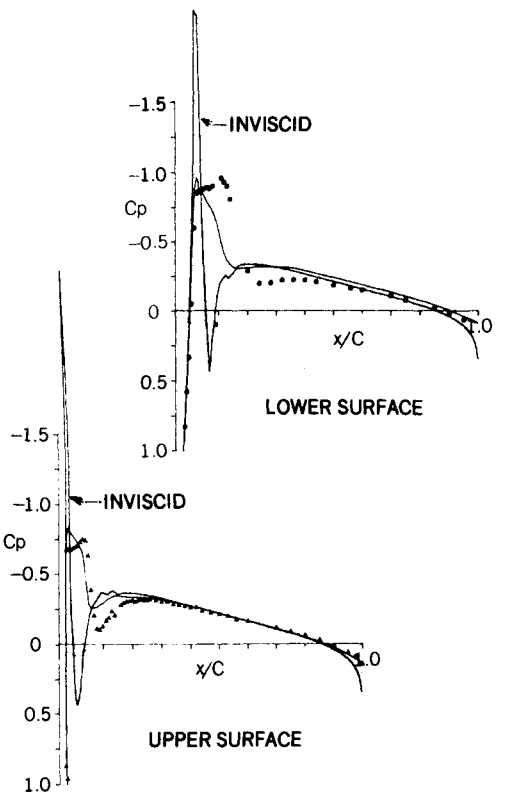


**a) $\alpha = 0$ deg**

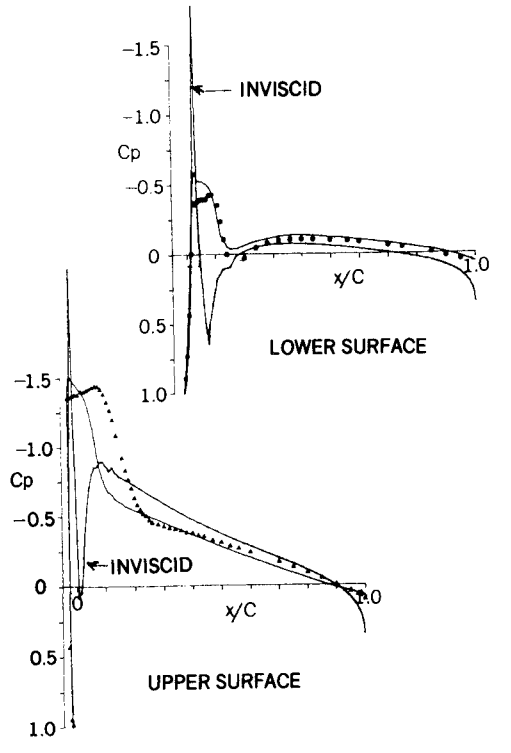


**b) $\alpha = 4$ deg**

**Fig. 16 Calculations and measurements of pressure coefficient at three angles of attack (second procedure with wake effect).**

he trailing edge is about 1% of the airfoil chord. This difference in the magnitudes of displacement thickness due to ice affects the pressure distribution and leads to a higher drag.

The results discussed in the previous paragraphs provide evidence of the ability of the first calculation method to represent the consequences of large accretions of ice. Since the calculations did not involve the wake, results have been confined to near-zero angles of attack. Figure 14 shows that the coefficients of lift and drag are in general agreement with experiment up to an angle of attack around 5 deg so that it can reasonably be expected that, even in the absence of the wake, the procedure is numerically satisfactory and provides useful results up to this angle. The wake has been incorporated in the

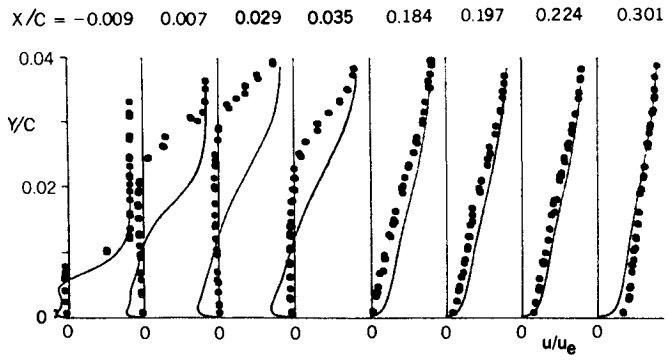


**Fig. 17 Profiles of mean velocity for the iced NACA 0012 airfoil at $R_c = 1.5 \times 10^6$ (second procedure with wake effect).**

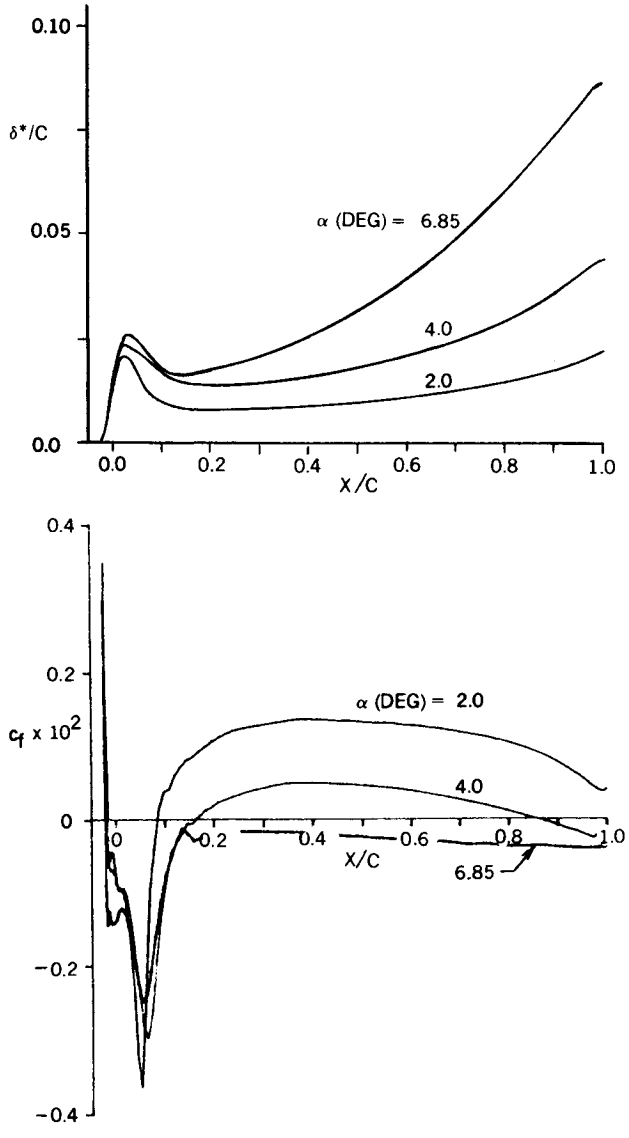


**Fig. 18 Influence of angle of attack on displacement thickness and skin-friction coefficient (second procedure with wake effect).**

calculations with the second procedure of Sec. II.C. Figure 15 presents distributions of the coefficients of lift and drag, which, as expected, are in better agreement with experiment and suggest that the iced airfoil will stall at an angle of attack of slightly less than 7 deg. This result confirms the viability of the second procedure and the importance of the wake at the higher angles of attack. It also shows that the effect of the ice has been to cause stall at an angle of attack of around half that associated with the clean airfoil.

Figures 16–18 presents additional results obtained with the second procedure and allow comparison with the measurements of Bragg and Spring.[6] The pressure coefficient distributions of Fig. 16 correspond to angles of attack of 0 and 4 deg and reveal several important features. It is evident that the calculated results have the same trends as the measurements and that the magnitude of the differences is larger than those usually associated with clean airfoils. In all cases, the discrepancies stem from the leading-edge region where strong pressure gradients and transition offer a considerable challenge to the calculation procedure. The inviscid flow results all show a rapid fall in the pressure coefficient to a minimum value that is considerably less than the measured value and demonstrates that they are of little value. Interaction with the viscous flow equations results in minimum values of pressure coefficient that are close to those of the measurements but occur further downstream. This feature of the calculated results is associated with the onset of transition, which was triggered by the initial fall in pressure coefficient and occurred upstream of the experimental transition. Further computational experiments are required to investigate this feature of the calculation method and to determine its influence on the downstream flow properties.

An example of the velocity profiles is provided by Fig. 17, which corresponds to the upper surface of the iced airfoil at 4 deg angle of attack and to the initial 30% of chord where the pressure coefficient distributions show discrepancies. As expected, these discrepancies are reflected in the profiles that incorrectly represent the magnitude of the size and velocities of the leading-edge separation bubble. It is clear from this result that the representation of transition will influence the separated flow and the length over which it exists; this, in turn, is likely to have a strong effect on the downstream flow. Care should be taken in interpreting Fig. 17 since the experimental techniques limit the accurate measurement of velocity to regions away from the separated flow bubble.

Figure 18 presents the variation of displacement thickness and skin-friction coefficient along the upper surface of the iced airfoil for angles of attack of 2, 4, and 6.85 deg. The rapid growth of displacement thickness from around 10% of chord is evident in the three cases with a threefold increase in the last case. The leading-edge bubble has increased from 10 to almost 20% of chord with increase in angles from 2 to 4 deg; at 6.85 deg, the flow is separated over the entire length of the surface so that stall will have occurred at a slightly lower angle. The results confirm the ability of this second procedure to deal with iced-airfoil flows at angles of attack up to and beyond stall.

## IV. Conclusions

The catastrophic effect of ice on the lifting characteristics of airplane components is evident from recent airplane accidents. Wind-tunnel experiments have confirmed that ice accretion can reduce the stall angle of a simple airfoil by a factor of two. This paper has shown that an efficient and convenient-to-use calculation method is able to represent the lift and drag characteristics of ice accurately and provides a basis for evaluating the consequences of ice accretion of different magnitudes and on a wide range of components. This method also is able to determine the flow properties on smooth and rough airfoils with accuracy similar to that of experiments and at considerably reduced cost.

The emphasis of the present paper has been on airfoils with surface roughness and ice accretion. In this context, the interactive boundary-layer procedure already is considerably less expensive than alternative methods based on higher-order forms of the Navier-Stokes procedures. These cost benefits are achieved without loss of accuracy. The procedure is readily extendable to three-dimensional geometries, including single and multielement wings, intakes, and empennages, where its low computer run times will be of even greater benefit.

In addition to extension of the present method to three-dimensional flows, further work is necessary to alleviate the sensitivity of the calculations to the rapid pressure changes of

the leading-edge region. Also, with the inclusion of the energy equation and consideration of the particle trajectories, a basis is available for the prediction of the shape of ice accretion as a function of position and time.

## Acknowledgment

This paper was prepared with the support of NASA Lewis Research Center, Icing Research Office Grant NAG3-601.

## References

[1]Gray, V. H. and Von Glahn, U. H., "Aerodynamic Effects Caused by Icing of an Unswept NACA 65A004 Airfoil," NACA TN-4155, 1957.

[2]Bragg, M. B. and Gregorek, G. M., "Wind Tunnel Investigation of Airfoil Performance Degradation Due to Icing," AIAA Paper 82-0582, March 1982.

[3]Bragg, M. B., Zaguli, R. J., and Gregorek, G. M., "Wind Tunnel Evaluation of Airfoil Performance Using Simulated Ice Shapes," NASA CR-167960, Nov. 1982.

[4]Korkan, K. D., Cross, E. J., and Cornell, C. C., "Experimental Aerodynamic Characteristics of an NACA 0012 Airfoil with Simulated Ice," *Journal of Aircraft,* Vol. 22, 1986, pp. 130–134.

[5]Bragg, M. B. and Coirier, W. J., "Detailed Measurements of the Flowfield in the Vicinity of an Airfoil with Glaze Ice," AIAA Paper 85-0409, Jan. 1985.

[6]Bragg, M. B. and Spring, S. A., "An Experimental Study of the Flowfield About an Airfoil with Glaze Ice," AIAA Paper 87-0100, Jan. 1987.

[7]Bragg, M. B. and Gregorek, G. M., "Predicting Aircraft Performance Degradation Due to Ice Accretion," Society of Automotive Engineers, Warrendale, PA, SAE Paper 83074, April 1983.

[8]Bragg, M. B., "Predicting Airfoil Performance with Rime and Glaze Ice Accretions," AIAA Paper 84-0106, Jan. 1984.

[9]Korkan, K. D., Dadone, L., and Shaw, R. J., "Performance Degradation of Helicopter Rotor Systems in Forward Flight Due to Rime Ice Accretion," AIAA Paper 83-0029, Jan. 1983.

[10]Shaw, R. J., "A Review of Techniques for Predicting Airfoil Performance in Icing," AIAA Paper 87-0028, Jan. 1987.

[11]Flemming, R. J. and Lednicer, D. A., "High Speed Ice Accretion on Rotorcraft Airfoils," NASA CR-3910, Aug. 1985.

[12]Cebeci, T., Clark, R. W., Chang, K. C., Halsey, N. D., and Lee, K., "Airfoils with Separation and the Resulting Wakes," *Journal of Fluid Mechanics,* Vol. 163, 1986, p. 323.

[13]Potapczuk, M. G. and Gerhart, P. M., "Progress in Development of a Navier-Stokes Solver for Evaluation of Iced Airfoil Performance," AIAA Paper 85-0410, Jan. 1985.

[14]Potapczuk, M. G., "Numerical Analysis of a NACA 0012 Airfoil with Leading Edge Ice Accretions," AIAA Paper 87-0101, Jan. 1987.

[15]Shaw, R. J., "Progress Toward the Development of an Aircraft Icing Analysis Capability," NASA TM-83562, 1984.

[16]Shaw, R. J., "NASA's Aircraft Icing Analysis Program," NASA TM-88791, 1986.

[17]Chang, K. C., Alemdaroglu, N., Mehta, U., and Cebeci, T., "Further Comparisons of Interactive Boundary-Layer and Thin-Layer Navier-Stokes Procedures," *Journal of Aircraft,* Vol. 25, Oct. 1988, pp. 897–903.

[18]Cebeci, T. and Smith, A. M. O., *Analysis of Turbulent Boundary Layers,* Academic Press, New York, 1974.

[19]Cebeci, T. and Bradshaw, P., *Physical and Computational Aspects of Convective Heat Transfer,* Springer-Verlag, New York, 1984.

[20]Bradshaw, P., Cebeci, T., and Whitelaw, J. H., *Engineering Calculation Methods for Turbulent Flows,* Academic Press, London, 1981.

[21]Abbott, I. H., von Doenhoff, A. E., and Stivers, L. S., "Summary of Airfoil Data," NACA Rept. 824, 1945.

[22]Cebeci, T. and Chang, K. C., "Calculation of Incompressible Rough-Wall Boundary-Layer Flows," *AIAA Journal,* Vol. 16, July 1978, pp. 730–735.

[23]Smith, A. M. O. and Kaups, K., "Aerodynamics of Surface Roughness and Imperfections," Society of Automotive Engineers, Warrendale, PA, SAE Paper 680198, April 1968.

[24]McGhee, R. J., Beasley, W. D., and Somers, D. M., "Low-Speed Aerodynamic Characteristics of a 13-Percent Thick Airfoil Section Designed for General Aviation Application," NASA TM-72697, 1977.